Int J Fract (2007) 148:415–433
DOI 10.1007/s10704-008-9213-7

ORIGINAL PAPER

Fracture assessment of U-notches under mixed mode loading: two procedures based on the 'equivalent local mode I' concept

F. Berto · P. Lazzarin · F. J. Gómez · M. Elices

Received: 31 October 2007 / Accepted: 28 April 2008 / Published online: 23 May 2008

Abstract Two fracture criteria are proposed and applied to blunt-notched components made of brittle materials loaded under mixed mode; the former is based on the averaged strain energy density over a given control volume, the latter on the cohesive crack zone model. In both instances use of the equivalent local mode I hypothesis is made. Only two material properties are needed: the ultimate tensile strength and the fracture toughness. Numerical predictions of rupture loads from the two criteria are compared with experimental measurements from more than 160 static tests with notched beams. The samples are made of PMMA and tested at −60°C to assure a bulk behaviour almost linear elastic up to rupture. Notch root radii range from 0.2 to 4.0 mm and load mixicity varies from pure mode I to a prevailing mode II. The good agreement between theory and experimental results adds further confidence to the proposed fracture criteria.

Keywords U-notches · Mixed mode · Local mode I · Strain Energy Density (SED) · Cohesive Zone Model (CZM)

F. Berto · P. Lazzarin
Department of Management and Engineering, University of Padova, Stradella S. Nicola 3, 36100 Vicenza, Italy

F. J. Gómez · M. Elices (✉)
Department of Materials Science, Universidad Politécnica de Madrid, E.T.S: Ingenieros de Caminos, 28040 Madrid, Spain
e-mail: melices@mater.upm.es

1 Introduction

Notches in structural components are weak points with a high risk of triggering brittle fracture; they may generate cracks or lead to fatigue crack initiation. When the notch is blunted (i.e. with a non-negligible root radius) and brittle fracture is expected, the conventional stress intensity factor cannot be applied, and a method to evaluate the maximum load that a component with a notch can sustain is needed.

Several criteria have been proposed to predict fracture loads of components with *notches*, subjected to *mode I loading* (See, for example Kipp and Sih 1975; Carpinteri 1987; Knésl 1991; Nui et al. 1994; Seweryn 1994; Gómez et al. 2000; Lazzarin and Zambardi 2001; Atzori and Lazzarin 2001; Strandberg 2002; Atzori et al. 2003, 2005; Gogotsi 2003; Leguillon and Yosibash 2003; Yosibash et al. 2004, 2006; Dini and Hills 2004; Taylor 2004; Lazzarin and Berto 2005a; Leguillon et al. 2007).

Recently, the authors successfully predicted fracture loads of notched specimens (sharp and blunted U and V notches) loaded under mode I, using two equivalent criteria; one based on the cohesive zone model (Gómez et al. 2000; Gómez and Elices 2003a,b, 2004), the other based on the local strain energy density (Lazzarin and Zambardi 2001; Lazzarin and Berto 2005a; Lazzarin et al. 2003, 2004, 2006, 2008; Livieri and Lazzarin 2005).

The problem of brittle failure from *blunted notches* loaded under *mixed mode* is more complex than in

mode I loading and experimental data, particularly for notches with a non- negligible radius, is scarce. Even so, several fracture criteria have been proposed (Papadopoulos and Paniridis 1988; Seweryn and Mróz 1995; Seweryn and Lucaszewicz 2002; Yosibash et al. 2006; Priel et al. 2007). In mode I, fracture systematically initiates from the notch tip located on the notch bisector line; this is the point where the main principal stress is at a maximum, as well as the maximum shear stress and the strain energy density. Conversely, the point where fracture starts in mixed mode varies from case to case, because it depends on the geometry of the notch and loading mode mixicity.

Fracture criteria based on a critical distance state that crack propagation occurs when the normal strain (McClintock 1958), or circumferential stress $\sigma_{\theta\theta}$ (Ritchie et al. 1973) at some critical distance from the crack tip, reaches a critical value. This "point criterion" becomes a "line criterion" in the papers by Knésl (1991) and Seweryn (1994) who dealt with components weakened by sharp V-shaped notches. Knéls and Seweryn formalised a stress criterion of brittle failure based on the assumption that crack initiation or propagation occurs when the mean value of the stress over a specified damage segment d_0 reaches a critical value. According to Knéls, d_0 is two to five times the grain size and then ranges for most metals from 0.03 mm to 0.50 mm. Seweryn denominated the segment d_0 "elementary increment of the crack length". Both authors quoted a previous paper by Novožhilov (1969). Afterwards, this critical distance-based criterion was extended also to structural elements under multi-axial loading (Seweryn and Mróz 1995; Seweryn et al. 1997) by introducing a non-local failure function combining normal and shear stress components, both normalised with respect to the relevant fracture stresses of the material.

The purpose of this paper is to generalise the previous results by the present authors for components with blunted notches loaded under mode I, to notched components loaded under mixed mode. This generalization is based on the hypothesis that fracture mainly depends on the local mode I and on the maximum value of the principal stress or the strain energy density.

The proposal of mode I dominance for cracked plates was suggested be Erdogan and Sih (1963) when dealing with cracked plates under plane loading and transverse shear, where the crack grows in the direction almost perpendicular to the maximum tangential stress in radial direction from its tip.

Two different methods are used to verify such a hypothesis: the cohesive zone model and the model based on the strain energy density over a control volume. Both methods allow us to evaluate the critical load under different mixed mode conditions when the material behaviour can be assumed as linear elastic.

Theoretical predictions were compared with more than 160 data from static tests performed on notched specimens taken from two recent contributions from the authors (Gómez et al. 2007a,b). All specimens were made of PMMA and tested at −60°C. In order to include a wide degree of experimental support to test the theoretical predictions, the experimental programme was carried out by changing specimen geometries, thus assuring a large range of loading modes (between pure mode I and almost pure mode II).

2 Summary of the experimental data

The material chosen for the experimental programme was polymethyl-methacrylate (PMMA) tested at −60°C, an amorphous glassy polymer that exhibits a non-linear behaviour at room temperature and linear elastic up to fracture at −60°C, even when tested without cracks or notches (Fig. 1) (Gómez et al. 2005). The average mechanical properties of PMMA at −60°C are shown in Table 1.

The experimental programme was performed with U-notched specimens, varying the notch inclination, the root radius and the boundary conditions.

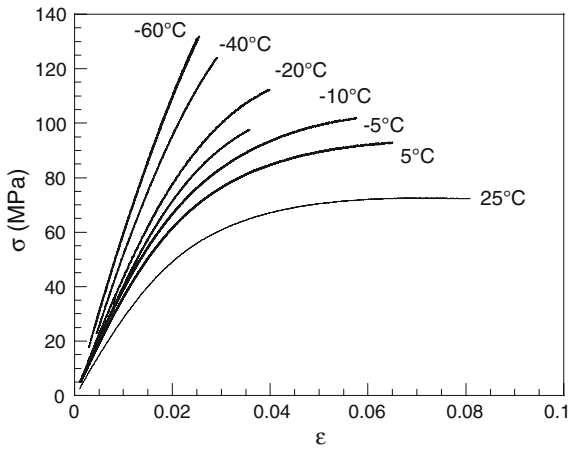

Fig. 1 Uniaxial stress–strain curve for PMMA at different temperatures

Table 1 Mechanical properties of PMMA at −60°C

Young's modulus	$E = 5.05 \pm 0.04$ GPa
Tensile strength	$\sigma_u = 128.4 \pm 0.1$ MPa
Fracture toughness	$K_{IC} = 1.7 \pm 0.1$ MPa m$^{1/2}$
Poisson's ratio	$\nu = 0.40 \pm 0.01$

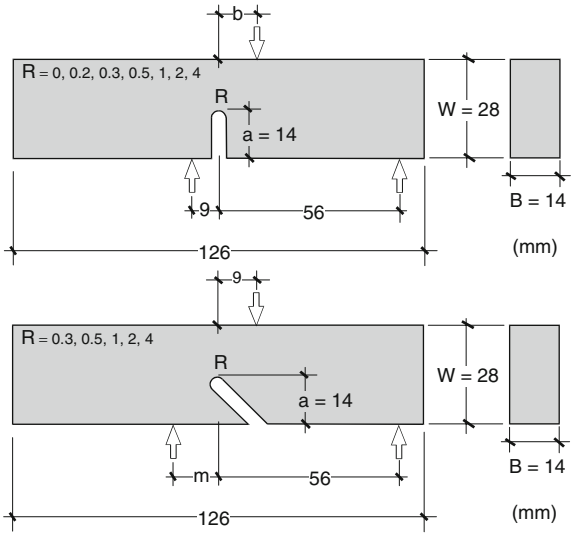

Fig. 2 Geometry and load condition. Data in mm ($b = -3$, 3, 9, 18, 27 and 36 mm; $m = 3$, 9 and 15 mm)

The geometries of the specimens are shown in Fig. 2. In all the specimens, the thickness, B, was 14 mm, the size, W, was 28 mm and the notch height, a, was 14 mm.

To achieve different mixed mode loading, two types of U-notched specimens were studied; beams with straight notches and beams with tilted notches, at 45°. Samples were loaded as shown in Fig. 2. When loading beams with straight notches, the position of the load point was modified; the distance from this point to middle point, b, was −3, 3, 9, 18, 27 and 36 mm. When loading beams with tilted notches, the position of the support was moved and the horizontal distance to the centre of the specimen, m, was 3, 9 and 15 mm.

The influence of the notch root radius, R, was examined by introducing seven different root radii. In the first straight notch series (characterised by $b = 9$, 18, 27 and 36 mm), R was 0, 0.2, 0.3, 0.5, 1.0, 2.0 and 4.0 mm. In the two series with $b = -3$ and 3 mm, as well as in the cases of tilted notches, the geometry with $R = 0.2$ mm was not considered. Three samples were tested for each configuration. All in all, 165 fracture tests were performed. Experimental details appear in the authors analysis (Gómez et al. 2007a,b), here only the critical loads for all the geometries are summarised in the Appendix. (Tables A1 and A2).

3 Fracture criterion based on the strain energy density averaged over a control volume

The concept of "elementary" volume and "micro structural support length" was introduced some time ago by Neuber (1958). Neuber formulated the idea that the material is sensitive to a fictitious root radius ρ_f, which was given according to the expression $\rho_f = \rho + s\varepsilon$ where ρ is the actual radius, s a factor that takes into account the state of multiaxility and ε the "micro structural support-length". This length depends on the material and not on the notch geometry, and was later correlated on its fracture toughness and ultimate tensile strength according to the expression $\varepsilon = (K_{\mathrm{Ic}}/\sigma_t)^2/(2\pi)$ (Neuber 1985).

Dealing here with the strain energy density concept, it is worthwhile contemplating some fundamental contributions provided by Sih and Gillemot. The concept of "core region" surrounding the crack tip was proposed by Sih (1973). The main idea is that the continuum mechanics stops short at a distance from the crack tip, providing the concept of the radius of the core region. The strain energy density factor S (Sih 1974a) was defined as the product of the strain energy density by a critical distance from the point of singularity. Failure was thought of as controlled by a critical value S_c, whereas the direction of crack propagation was determined by imposing a minimum condition on S.

The theory was extended to employ the total strain energy density near the notch tip (Sih 1974b), and the point of reference was chosen to be the location on the surface of the notch where the maximum tangential stress occurs. This was due to expectation that from this point fracture will proceed, although failure loads based on this stress are not satisfactory.

The strain energy density fracture criterion was refined and extensively summarised in chapter 5 of Sih's book (Sih 1991). The material element is always kept at a finite distance from the crack or the notch tip outside the "core region" where the inhomogeneity of the material due to micro-cracks, dislocations and grain boundaries precludes an accurate analytical solution. The theory can account for yielding and fracture and is

applicable also to ductile materials. Depending on the local stress state, the radius of the core region may or may not coincide with the critical ligament r_c that corresponds to the onset of unstable crack extension (Sih 1991, chapter 8). The ligament r_c depends on the fracture toughness K_{IC}, the yield stress σ_y, the Poisson's ratio ν and, finally, on the ratio between dilatational and distortional components of the strain energy density. The direction of S_{max} determines maximum distortion while S_{min} relates to dilatation. Distortion is associated with yielding, dilatation tends to be associated to the creation of free surfaces or fracture and occurs along the line of expected crack extension (Sih 1991, Chapter 5).

A critical value of strain energy density function $(dW/dV)_c$ has been extensively used also by Gillemot and collaborators (Gillemot 1965, 1976; Czoboly et al. 1982; Gillemot et al. 1985), who determined experimentally $(dW/dV)_c$ for various engineering materials by using plain and notched specimens. The deformation energy required for crack initiation in a unit volume of material is termed Absorbed Specific Fracture Energy (ASFE) by Gillemot, who also discussed its links with the critical value of J_c and the critical factor S_c. This subject was considered also by Sih who showed that $(dW/dV)_c$ is equivalent to S_c/r, where S_c is the critical strain energy density factor and the radius vector r identifies the location of failure (Sih 1974b, 1991).

Since distributions of the absorbed specific energy W in notched specimens are not uniform, Gillemot assumed that the specimen cracks as soon as a precise energy amount has been absorbed by the small plastic zone at the root of the notch. If the notch is sufficiently sharp, specific energy due to the elastic deformation is small enough to be neglected as an initial approximation (Gillemot 1976).

While measurements of the energy in an infinitely small element are not possible, they can be approximated with sufficient accuracy by calculating the fracture energy over the entire fractured cross section of an unnotched tensile specimen (Gillemot et al. 1985). Notched components loaded under static loads show that the average ASFE decreases with increasing the notch sharpness, with the ASFE parameter being plotted as a function of the theoretical stress concentration factor, K_t, and the temperature (Gillemot et al. 1985).

For a common welded structural steel and $K_t = 1$, the ASFE value, obtained by tensile tests, is about $1.0\,MJ/m^3$ while for values of K_t greater than 3.0 a plateau value is visible (Gillemot et al. 1985). Depending on the considered welded metal, the plateau approximately ranges between 0.15 and $0.35\,MJ/m^3$. These values are not so different from the mean value that characterises the high cycle fatigue strength of welded joints, $\Delta W_C = 0.105\,MJ/m^3$ but with reference to a specific control volume (Lazzarin et al. 2003; Livieri and Lazzarin 2005).

Dealing here with control volumes applied to notched components, it is worth mentioning that the idea of averaging over a finite size volume was examined in a paper by Sheppard, who quantified the stress state in the volume by means of a single parameter, the average value of the circumferential $\sigma_{\theta\theta}$ stress (Sheppard 1991). The volume was a semicircular sector whose radius could exactly be evaluated by using the finite element method. The radius was varied until the resulting value of K_f, thought of as coincident with the averaged stress to nominal stress ratio, matched the experimental data for a particular notch geometry (Sheppard 1991).

Different from Sih's criterion, which is a point-related criterion, the averaged strain energy density criterion (SED) as reported in (Lazzarin and Zambardi 2001; Yosibash et al. 2004) states that brittle failure occurs when the mean value of the strain energy density over a control volume (which becomes an area in two dimensional cases) is equal to a critical energy W_c. The SED approach is based both on a precise definition of the control volume and the fact that the critical energy does not depend on the notch sharpness. Such a method was formalised and applied first to sharp, zero radius, V-notches and later extended to blunt U- and V-notches under Mode I loading (Lazzarin and Berto 2005a). The authors argue that the extension of the SED approach to ductile fracture is possible, with a major problem being the definition of the control volume and the influence of the dilatational and distortional components of the strain energy density. In such a case, it should be remembered that in referring to small-scale yielding, Ellyin and Kujawski extended to cyclic loading of notched components a method based on the averaged of the stress and strain product within the elastic-plastic domain around the notch (Ellyin and Kujawski 1989; Ellyin 1997).

Recently, the effect of plasticity in terms of strain energy density over a given control volume has been considered by the present authors, showing different behaviours under tension and torsion loading, as well as under small and large scale yielding (Lazzarin and Berto 2008).

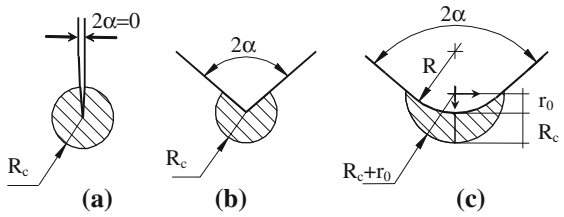

Fig. 3 Critical volume definition for crack (**a**), sharp V-notch (**b**), and blunt V-notch (**c**) under mode I loading

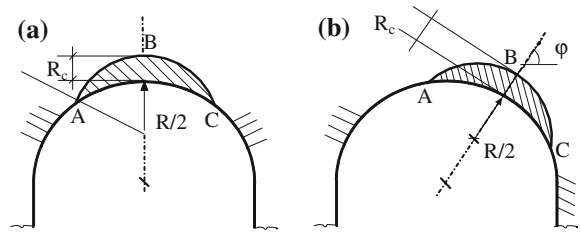

Fig. 4 Critical volume in U-notches under mode I (**a**) and mixed mode loading (**b**)

When dealing with cracks the critical volume is a circle of radius R_c centred at the tip (Fig. 3a). For a sharp V-notch, the critical volume becomes a circular sector of radius R_c centred at the notch tip (Fig. 3b). Finally, for a blunt V-notch under mode I loading, the volume assumes the crescent shape shown in Fig. 3c, where R_c is the depth measured along the notch bisector line. The total radius of the crescent shape is greater, equal to $R_c + r_0$, being r_0 a distance that depends on the V-notch opening angle 2α, according to the expression $r_0 = \mathrm{R}(\pi - 2\alpha)/(2\pi - 2\alpha)$ (Lazzarin and Tovo 1996). For U-notches $\mathrm{r_0}$ is simply equal to R/2, as in Creager-Paris' equations for blunt-cracks (Creager and Paris 1967). The link between the total strain energy over the particular control volume and Rice's J-integral was discussed by Berto and Lazzarin (2007) for U- and V-shaped notches under mode I loading.

To apply this fracture criterion, two independent parameters are needed: the critical value of the strain energy density, W_c, and the critical length, R_c. For an ideally linear elastic material

$$W_c = \frac{\sigma_u^2}{2E} \tag{1}$$

being σ_u the ultimate tensile stress and E the elastic modulus. The critical length, R_c, can be evaluated according to the following expressions:

$$R_c = \frac{(1+\nu)(5-8\nu)}{4\pi}\left(\frac{K_{IC}}{\sigma_u}\right)^2. \tag{2a}$$

under plane strain conditions (Yosibash et al. 2004), K_{IC} being the fracture toughness and ν the Poisson's ratio, or

$$R_c = \frac{(5-3\nu)}{4\pi}\left(\frac{K_C}{\sigma_u}\right)^2 \tag{2b}$$

under plane stress conditions (Lazzarin and Berto 2005b). The two independent parameters for PMMA at −60°C are, taking into account Eqs. 1 and 2a and Table 1 values, $W_c = 1.6\,\mathrm{MJ/m^3}$, and $R_c = 0.035\,\mathrm{mm}$

The critical volume in U-notched specimens under mode I loading conditions is centred in relation to the notch bisector line (Fig. 4a). Under mixed mode loading the critical volume is no longer centred on the notch tip, but rather on the point where the principal stress reaches its maximum value along the edge of the notch (Fig. 4b). It is assumed that the crescent shape volume rotates rigidly under mixed mode, with no change in shape and size. (Gómez et al. 2007a). This is the governing idea of the '*equivalent local mode I*' approach, as proposed in this research.

The maximum stress occurring along the edges of U-notches has been calculated numerically by using the FE code ANSYS 9.0®. For each geometry two models were created: the first was mainly oriented to the determination of the point where the maximum principal stress was located; the second model was more refined, with an accurate definition of the control volume where the strain energy density should be averaged. All the analyses have been carried out by means of eight-node elements under plane strain and linear-elastic hypotheses. Figures 5, 6, and 7 show the maximum principal stress and the strain energy density contour lines inside the control volume for the three configurations with different m values. The strain energy density is approximately symmetric in relation to the ideal line normal to the edge and crossing the point of the maximum principal stress. The main results of the FE analyses are reported in Tables A3 and A4.

For blunted notches loaded in *mode I*, the averaged value of the strain energy density, $\overline{W}_1^{(e)}$, can be expressed as (Lazzarin and Berto 2005a):

$$\overline{W}_1^{(e)} = H(R_c/R)\,\frac{\pi\sigma_{\max}^2}{4E} \tag{3}$$

where σ_{max} is the maximum stress at the notch tip and H is a parameter that depends on the normalised radius R/R_c and the Poisson's ratio ν. H condenses the contribution of all stresses and strains present on the control

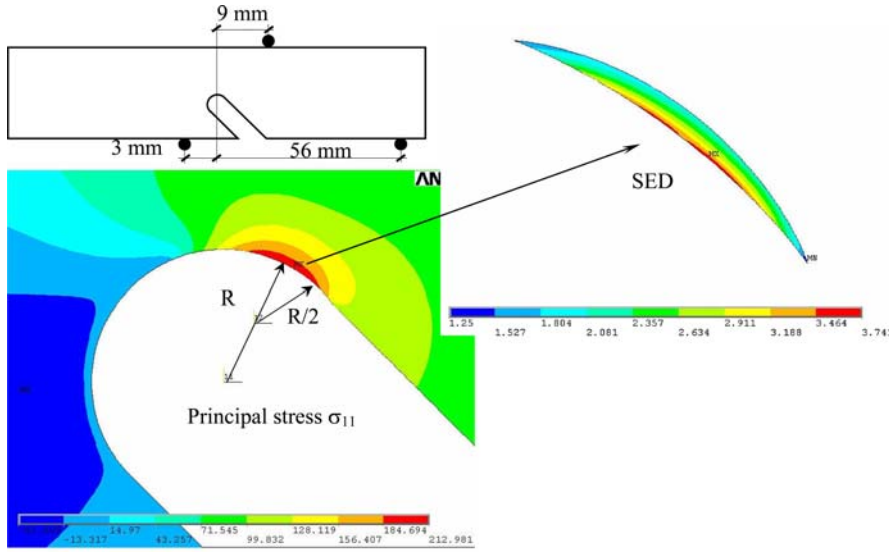

Fig. 5 Principal stress and strain energy density contour lines for the case $R = 0.3\,\text{mm}$ and $m = 3\,\text{mm}$

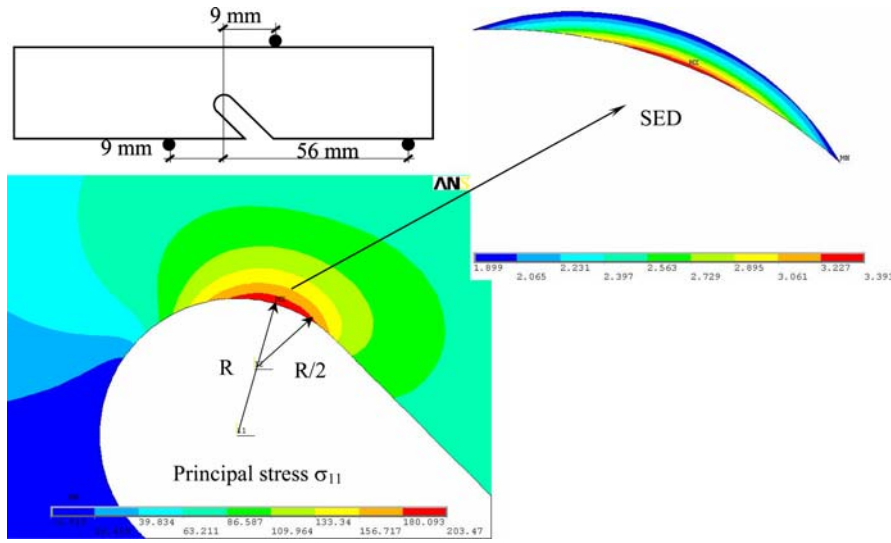

Fig. 6 Principal stress and strain energy density contour lines for the case $R = 0.3\,\text{mm}$ and $m = 9\,\text{mm}$

volume, its analytical expression appears in a Lazzarin and Berto analysis (Lazzarin and Berto 2005a). Table 2 gives the values for H corresponding to Mode I, plain strain conditions with, $\nu = 0.4$ and $R_c = 0.035\,\text{mm}$.

For *mixed mode* loading an equivalent expression for the averaged strain energy density is proposed:

$$\overline{W}^{(e)} = H^*(R_c/R)\,\frac{\pi\left(\sigma^*_{\max}\right)^2}{4E} \tag{4}$$

where $\sigma^*_{\max}$ is the maximum value of the principal stress along the notch edge and H^* depends again on the normalised radius R/R_c, the Poisson's ratio ν and the loading conditions. Values of H^* are listed in the Table 2 and compared with the corresponding values of H. It is evident that the dependence on the loading conditions is weak for all the straight notches, the difference between H and H^* being less than 1%. The difference increases to 8.5% in the case of two tilted notches ($m = 3\,\text{mm}$, $R = 0.3\,\text{mm}$ and $0.5\,\text{mm}$), being less than 5% in the other 13 cases.

Based on this result, an approximate procedure to evaluate the critical load, P_{cr}, under mixed mode loading once σ^*_{max} is known, is by using the following equation:

$$\overline{W}^{(e)}_{cr} = H(R_c/R)\,\frac{\pi\left[\sigma^*_{\max}\left(P_{cr}\right)\right]^2}{4E} \tag{5}$$

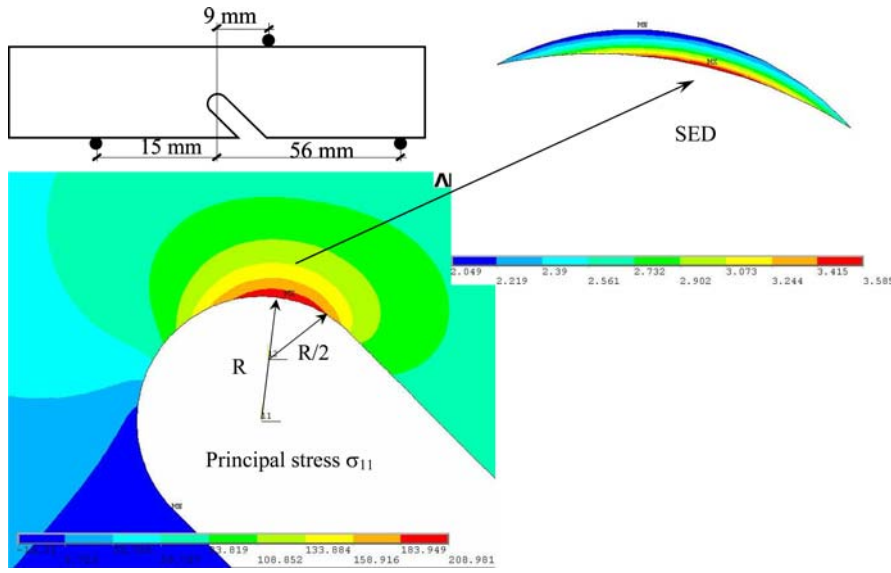

Fig. 7 Principal stress and strain energy density contour lines for the case $R = 0.3$ mm and $m = 15$ mm

where in Eq. 4, H^* was changed by H. Some plots of the stress components ($\sigma_{\theta\theta}$, σ_{rr}, and $\sigma_{r\theta}$) are shown in Fig. 8 where two root radii, $R = 0.3$ and 4.0 mm, corresponding to a tilted notch with $m = 3$ mm, are considered. Stresses in cylindrical coordinates are plotted over a line perpendicular to the notch edge, drawn over the point of maximum principal stress. Under mode I conditions, the shear stress component $\sigma_{r\theta}$ is always equal to zero ahead of the notch tip. Under mixed mode conditions, $\sigma_{r\theta}$ is practically zero for $R = 4.0$ and, in both cases, very low in comparison with the hoop stress, particularly near the notch edge. The concept of *equivalent local mode I*, although not exact in principle, can be seen as an accurate engineering approximation.

In the Erdogan-Sih criterion, valid for cracks, the angle of maximum tangential stress was obtained by imposing equal to zero the shear angular function (Erdogan and Sih 1963). By using plexiglass plates weakened by a crack under pure shear loading, Erdogan and Sih showed that the fracture angle varied around 70° with very small scatter. That angle was in agreement with the theoretical assessment (70.5° in absolute value) obtained in the skew-symmetric case.

Considering mode I loading conditions, some relationships between J-integral and the strain energy evaluated in a given finite size volume, surrounding the tip of sharp and blunt V-notches, were recently presented (Berto and Lazzarin 2007). With the aim of assessing the static failure of specimens weakened by U-notches, an attempt was carried out to link the strain energy density $\bar{W}$ averaged over a control volume and the J-integral as determined on the inner arc delimitating the same semi-moon-like volume (i.e. the arc $(\widehat{ABC})$ as shown in Fig. 4). This allowed the researchers to create a link among J-integral, the mean value of the strain energy density $\bar{W}$ and the material-dependent control radius R_c.

Many attempts have been made in the past to study the problem of crack growth under mixed mode loading by using path-independent line integrals (see Gdoutos 1990). The J-integral, as proposed by Rice (1968), is the first component of the vector J_k ($k = 1, 2$), as defined in (Knowles and Sternberg 1972; Budiansky and Rice 1973):

$$J_k = \int_\Gamma \left(W n_k - T_i \cdot \frac{\partial u_i}{\partial x_k} ds \right) \quad (k = 1, 2) \tag{6}$$

where W is the strain energy density, n_k is the unit normal vector to the contour Γ, where J is evaluated, and u_i and T_i are the components of the displacement and traction vectors, respectively. In a less synthetic form, J_1 and J_2 can be expressed as follows:

$$J_1 = \int_\Gamma \left[W n_1 - (\sigma_{xx} n_1 + \tau_{xy} n_2) \frac{\partial u_x}{\partial x_1} - (\tau_{xy} n_1 + \sigma_{yy} n_2) \cdot \frac{\partial u_y}{\partial x_1} \right] ds \tag{7a}$$

Table 2 Numerical values for H and H^* ($R_c = 0.035$ mm)

R (mm)	H	H^* (straight notches)						H^* (inclined notches)			
		$b = -3$ (mm)	$B = 3$ (mm)	$b = 9$ (mm)	$b = 18$ (mm)	$b = 27$ (mm)	$b = 36$ (mm)	$m = 15$ (mm)	$m = 9$ (mm)	$m = 3$ (mm)
0.2	0.3459	–	–	0.3459	0.3508	0.3459	0.3459	–	–	–
0.3	0.3940	0.3888	0.3897	0.3940	0.3940	0.3940	0.3940	0.3903	0.3790	0.3629
0.5	0.4416	0.4419	0.4391	0.4436	0.4458	0.4416	0.4463	0.4403	0.4315	0.4067
1.0	0.4843	0.4846	0.4839	0.4819	0.4884	0.4843	0.4843	0.4826	0.4784	0.4617
2.0	0.5085	0.5093	0.5119	0.5061	0.5085	0.5055	0.5085	0.5043	0.5030	0.4952
4.0	0.5213	0.5250	0.5238	0.5156	0.5186	0.5213	0.5213	0.5193	0.5172	0.5135

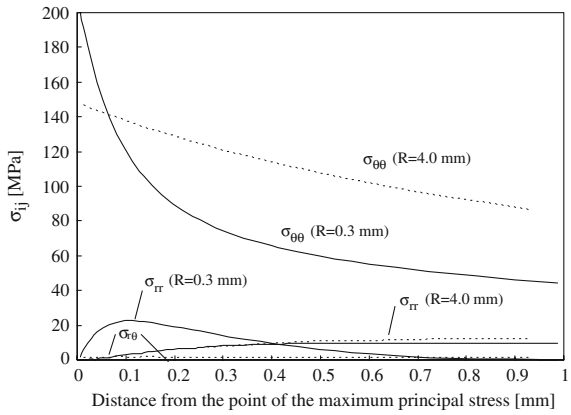

Fig. 8 Stress components plotted against the distance from the point on the notch edge where the maximum principal stress reaches its maximum value

$$J_2 = \int_{\Gamma} \left[W n_2 - (\sigma_{xx} n_1 + \tau_{xy} n_2) \frac{\partial u_x}{\partial x_2} - (\tau_{xy} n_1 + \sigma_{yy} n_2) \cdot \frac{\partial u_y}{\partial x_2} \right] ds \tag{7b}$$

Chen and Lu (2004) analysed the path dependence of the J_k-vector when applied to the circular arc of blunt U- and V-notches. They found a new condition to ensure the path-independence of the J-integral, based on the zeroing of the projected contributions from the J_2 integral evaluated in local coordinate system along the integration path (traction-free surfaces). Moreover, they underlined the importance played by J_2 in studying fracture of notch-like defects.

Following the guidelines drawn for U-notches in mode I loading, a new proposal for the use of the J-integral in mixed mode is presented here. When mixed mode conditions are present, both J_1 and J_2 are different from zero; the modulus of the vector J_k can be evaluated by using the expression

$$J_{eq} = \sqrt{J_1^2 + J_2^2} \tag{8}$$

Considering that now the same rotated volume as defined for the SED evaluations ($R_c = 0.035$ mm), it is possible to define the averaged value of J_{eq} over the arc defined by points A, B and C, which describes the inner perimeter of the selected volume (see Fig. 4b):

$$J_{arc} = \frac{J_{eq}}{arc(\widehat{ABC})} \tag{9}$$

For the beams with tilted notches, which presented the higher contribution due to mode II, Table 3 lists the

Table 3 Application of the J-integral to beams with tilted notches and comparison with the SED

R (mm)	m (mm)	J_1 (N/mm)	J_2 (N/mm)	J_{eq} (N/mm)	arc (mm)	$J_{arc} = J_{eq}$/arc (Nmm/mm^3)	SED (Nmm/mm^3)
4	15	1.88	0.71	2.01	1.08	1.86	1.91
	9	1.74	0.80	1.92	1.08	1.77	1.78
	3	1.57	0.99	1.86	1.08	1.72	1.75
2	15	1.49	0.56	1.59	0.76	2.09	2.08
	9	1.40	0.61	1.53	0.76	2.01	1.96
	3	1.34	0.82	1.57	0.76	2.07	2.06
1	15	1.15	0.30	1.19	0.56	2.12	2.13
	9	1.07	0.42	1.15	0.56	2.05	2.07
	3	0.99	0.58	1.15	0.56	2.05	2.06
0.5	15	0.81	0.17	0.83	0.42	1.97	1.98
	9	0.68	0.23	0.72	0.42	1.71	1.83
	3	0.74	0.66	0.99	0.42	2.36	2.18
0.3	15	0.91	0.11	0.92	0.34	2.70	2.65
	9	0.82	0.34	0.89	0.34	2.61	2.44
	3	0.77	0.38	0.86	0.34	2.53	2.56

values of J_1, J_2, J_{eq} and J_{arc}. The results are reported for the three different values of the span length m already considered in the experimental programme and for all the values of the notch root radius R. In addition, a comparison between the values of J_{arc} (as obtained by averaging the modulus of the J_k-vector over the perimeter of the control volume) and the SED is presented. The agreement between the two parameters is accurate also for mixed mode loading, as has already occurred in the pure mode I case. This provides not only a new interpretative key to J when applied to blunt notches under mixed mode loading (I+II), but also confirmation that J_{arc} is a worthy engineering tool for static assessment of components weakened by U-notches.

It is important to note that J_{arc} is not rigorously formulated and precisely defined for the crack case (see also Berto and Lazzarin 2007 and Berto et al. 2007). In fact, the definition of R_c has not been updated with respect to the definition based on the SED approach. Furthermore, it should also be highlighted that dealing with a blunt notch the J-integral is path-dependent and the only way to extend its use, as an assessment parameter, in the case of finite value of the notch radius is to define a characteristic length dependent on the material. This length, conceptually similar to the microstructural support length introduced first by Neuber (1958, 1985), "decides" on which path J has to be evaluated (Livieri 2008). The SED approach allows to take into account the averaged energy in an area, while the J_{arc} gives the value of the line energy averaged along a characteristic path (in this case the path is defined as the perimeter of the control volume and is then tied to R_c). Two different energetic approaches—one rigorously formulated and analytically developed, and another based on the control radius defined by means of SED criterion—give the same results because they are conceptually linked.

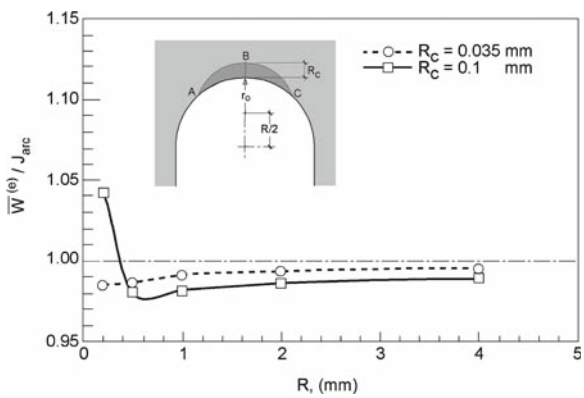

Fig. 9 Ratio between the SED and J_{arc}, as a function of notch root radius R, for two different R_c values

The ratio β between the SED and J_{arc}, as a function of the notch root radius R, is plotted in Fig. 9 for

two different values of the control radius R_c (0.035 and 0.1 mm) showing that, despite the approximate definition of J_{arc}, β is near to 1, confirming our engineering choice.

4 Fracture criterion based on the cohesive zone model

The cohesive model was first proposed in the 1960s by Dugdale (1960) and Barenblatt (1962) from a theoretical point of view to eliminate the stress singularity at the tip of the crack. In the 1970s, Hillerborg et al. (1976) generalised the cohesive zone (CZM) model to explain fracture process where no initial macroscopic crack existed. This last generalization is the starting point for applying this model to notches. A review of this model, together with some improvements, was made by the authors in a recent paper (Elices et al. 2002).

The material is characterised by the properties of the bulk material and by the conditions for the initiation and development of cracking. A cohesive crack initiates at the point where the maximum principal stress σ_{11} first reaches a critical value, being termed the cohesive stress f_t. This cohesive crack initiates in the direction perpendicular to the maximum principal stress. After its formation, the cohesive crack opens while transferring stress from one face to the other one. The transferred stress strictly depends on the crack opening displacement. For a monotonic load and local mode I, the stress transferred σ, is normal to the crack faces and is a unique function of the crack opening w. The material function linking σ and w is termed the softening function.

The material behaviour is characterised by the constitutive equations of the bulk material and the softening function. In this research, the bulk material behaviour is assumed linear elastic and the softening function a rectangular law, in accordance with previous results (Gómez et al. 2005).

The rectangular softening function has been successfully employed for PMMA at −60°C where fracture assessment of notches in mode I was the prime concern (Gómez et al. 2005). This softening curve is the simplest one and depends only on two parameters: the cohesive stress f_t and the fracture energy G_F. Here, the cohesive stress f_t is assumed as equal to the tensile strength measured at −60°C from unnotched specimens, while the fracture energy was calculated from the knowledge of the fracture toughness and Eq. 10.

$$G_F = \frac{K_{IC}^2}{E'} \tag{10}$$

where $E' = E/(1-\nu^2)$. By using the mechanical properties shown in Table 1, such a softening function of PMMA was characterised by $f_t = 128$ MPa and $G_F = 480$ N/m.

In mode I loading, the geometry and loading is symmetrical to the symmetry plane of the notch. This has the advantage of knowing, a priori, the crack path as well as the plane on which the cohesive process zone develops, and allows us to model only half of the geometry. The cohesive process zone is modelled on this plane as a mixed boundary condition by stipulating a relationship between stresses and displacements given by the softening function.

In mixed mode loading the problem is more complex, given that the fracture path is initially unknown. This problem could be overcome by using the local mode I approach, with the hypothesis that the cohesive crack initiates ahead of the notch in the point where the principal stress reaches its maximum value. It could then be analysed by placing close to this point, perpendicular to the notch edge, a band of cohesive elements, where the behaviour is defined by the softening function in a similar manner to in Mode I. To improve slightly this procedure, a triangle of special elements is placed near the critical point, allowing a possible curvature in the initial path of the cohesive crack.

Calculations were performed with the freeware finite element code COFE, developed in the Department of Materials Science at the Universidad Politécnica de Madrid (Planas and Sancho 2007). The local mode I hypothesis allows us to determine the initial position of the cohesive crack: the point at the notch boundary where the main elastic principal stress is at a maximum. After a first linear elastic calculation to reach such a point, an isosceles triangle was placed over it with the height of the triangle perpendicular to the notch, to simulate the cohesive crack. The general form of all the FE meshes appears in Fig. 10. The size of the element decreases near the critical point on the notch up to 4 μm. Special cohesive elements had been placed into the triangular area, using the embedded crack technique (Sancho et al. 2007). Bulk elements are conventional linear triangular plane strain elements. Calculations were performed controlling the displacement of the node at the cohesive crack initial point.

This procedure predicts the maximum load when the maximum displacement between the lips of the

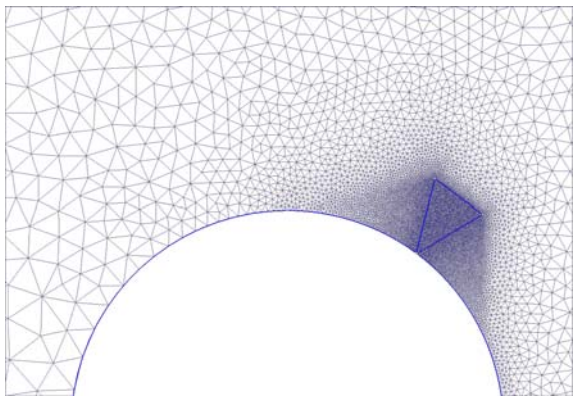

Fig. 10 Detail of the mesh used in cohesive calculations ($R = 1\,\text{mm}$)

cohesive crack reaches the critical value, w_c, equal to the fracture energy divided by the cohesive stress f_t. When the problem is formulated analytically and an actual crack is considered, two equations govern fracture: the maximum displacement among the cohesive crack lips and the fact that the stresses are finite near the cohesive crack. Thus, the stress intensity factor must be equal to zero, i.e.:

$$w_c = \frac{G_F}{f_t} \tag{11}$$

and

$$K_I = 0 \tag{12}$$

Using the superposition principle, the initial state can be analysed as a combination of two auxiliary states, shown in Fig. 11: a loaded notched sample, having a crack without transferring stresses and a notched sample without external loads and with a crack loaded by cohesive forces. Introducing this concept into Eqs. 11, 12 one reaches at:

$$\frac{G_F}{f_t} = C_P\left(a_{cohesive}, geometry\right) R \frac{P_{cr}}{BDE'} - C_f\left(a_{cohesive}, geometry\right) R \frac{f_t}{E'} \tag{13}$$

$$0 = g_P\left(a_{cohesive}, geometry\right) \sqrt{R} \frac{P_{cr}}{BD} - g_f\left(a_{cohesive}, geometry\right) f_t \sqrt{R} \tag{14}$$

In expressions (13) and (14) the first term corresponds to state I (see Fig. 11) and the second to state II (Fig. 11). C_P and C_f are dimensionless stiffness functions (which depend on the geometry and the size of the

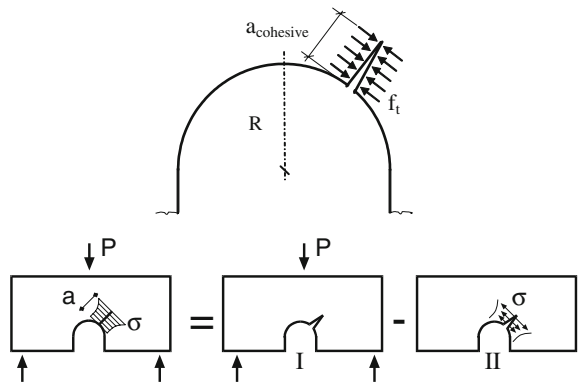

Fig. 11 Cohesive crack and superposition diagram

cohesive crack, $a_{cohesive}$) B and D, two dimensions of the sample, and g_P and g_f the dimensionless shape functions. A general description of these two equations and the procedure can be found in Bažant and Planas (1998). After solving the equation system, one obtains P_{cr} and $a_{cohesive}$, where

$$a_{cohesive} = a_{cohesive}\left(\frac{R}{l_{ch}}, geometry\right), \quad P_{cr} = P_{cr}\left(\frac{R}{l_{ch}}, geometry\right) \tag{15}$$

and l_{ch} a material characteristic length (Hillerborg et al. 1976) defined as

$$l_{ch} = \frac{E' G_F}{f_t^2} \tag{16}$$

Rearranging expression (15) in a dimensionless form, the system of equations provides the following relationship

$$\frac{G_F}{f_t} = \frac{P_{cr}}{BDE'} Rf\left(\frac{R}{l_{ch}}\right) \tag{17}$$

For notched components under *mode I* loading, Eq. 17 can be modified, taking into account the maximum stress at the notch edge and the new function h, as:

$$\frac{G_F}{f_t} = \frac{\sigma_{MAX}}{E'} Rh\left(\frac{R}{l_{ch}}\right) \tag{18}$$

This equation can be further modified by considering the ratio t_k between the σ_{max} and the critical load P_{cr}, as:

$$\frac{G_F}{f_t} = \frac{t_k P_{cr}}{E'} Rh\left(\frac{R}{l_{ch}}\right) \tag{19}$$

The numerical values of the function h corresponding to mode I are shown in Table 4. For *mixed mode* loading, an analogous expression can be stated as:

$$\frac{G_F}{f_t} = \frac{t_k^* P_{cr}}{E'} Rh^*\left(\frac{R}{l_{ch}}\right) \tag{20}$$

where, again, t_k^* is the ratio between the maximum stress at the notch and the applied load, and h^* is a function of the normalised radius, R/l_{ch}, of the geometry and the loading conditions. The parameter h^* has been calculated and shown in Table 4 for $l_{\mathrm{ch}} = 0.176$ mm, the characteristic length for PMMA. The values of Table 4 show that the dependence of h and h^* from the loading modes is weak.

Involving the same reasoning as in the SED criterion, an approximate procedure is proposed to evaluate the critical load, P_{cr}, in mixed mode loading by substituting h^* by h, as both values are almost equal. The resulting equation is:

$$\frac{G_F}{f_t} = \frac{t_k^* P_{cr}}{E'} Rh\left(\frac{R}{l_{ch}}\right) \tag{21}$$

This simple formula provides accurate predictions, as shown in the next section.

5 Comparison of experimental results with numerical predictions

The experimentally measured critical loads from the 160 tests, performed with notched beams loaded under mixed mode, are compared with the numerical predictions based on the SED and CZM criteria. The critical loads, deduced from Eqs. 5 and 21 are given by

$$P_{cr} = \frac{2}{t_k^*}\sqrt{\frac{E\bar{W}_{cr}^{(e)}}{\pi H(R_c/R)}} \tag{22}$$

for the SED criterion and by

$$P_{cr} = \frac{E'G_F}{f_t t_k^* Rh\left(\frac{R}{l_{ch}}\right)} \tag{23}$$

when the CZM criterion is used.

To calculate these critical loads, one needs to know some material properties obtained from two tests: a tensile test and a fracture toughness test. The ratio t_k^*, can be extracted from linear elastic calculations and the functions h and H, are given in Tables 2 and 4.

Figures 12 and 13 compare the *experimental* values of the critical loads as a function of the notch root radius with the *numerical* predictions based either on the CZM model or the SED model, as well as with those based on the two simplified procedures, Eqs. 5 and 21. Figure 12 corresponds to the straight notches, each one with a different value of b; Fig. 13 corresponds to the inclined notches, with different values of m. The agreement is found to be satisfactory for the SED model and accurate

Table 4 Numerical values for h and h^* ($l_{\mathrm{ch}} = 0.176$ mm)

R (mm)	h	H^* (straight notches)						h^* (inclined notches)		
		$b = -3$ (mm)	$b = 3$ (mm)	$b = 9$ (mm)	$b = 18$ (mm)	$b = 27$ (mm)	$b = 36$ (mm)	$m = 15$ (mm)	$m = 9$ (mm)	$m = 3$ (mm)
0.2	0.5136	–	–	0.5175	0.5197	0.5221	0.5150	–	–	–
0.3	0.3752	0.3802	0.3794	0.3754	0.3757	0.3760	0.3763	0.3788	0.3764	0.3685
0.5	0.2470	0.2456	0.2455	0.2449	0.2471	0.2464	0.2498	0.2488	0.2467	0.2415
1.0	0.1361	0.1349	0.1359	0.1371	0.1355	0.1357	0.1357	0.1365	0.1354	0.1343
2.0	0.0733	0.0723	0.0726	0.0726	0.0728	0.0729	0.0728	0.0727	0.0725	0.0718
4.0	0.0383	0.0376	0.0377	0.0380	0.0378	0.0380	0.0380	0.0381	0.0380	0.0379

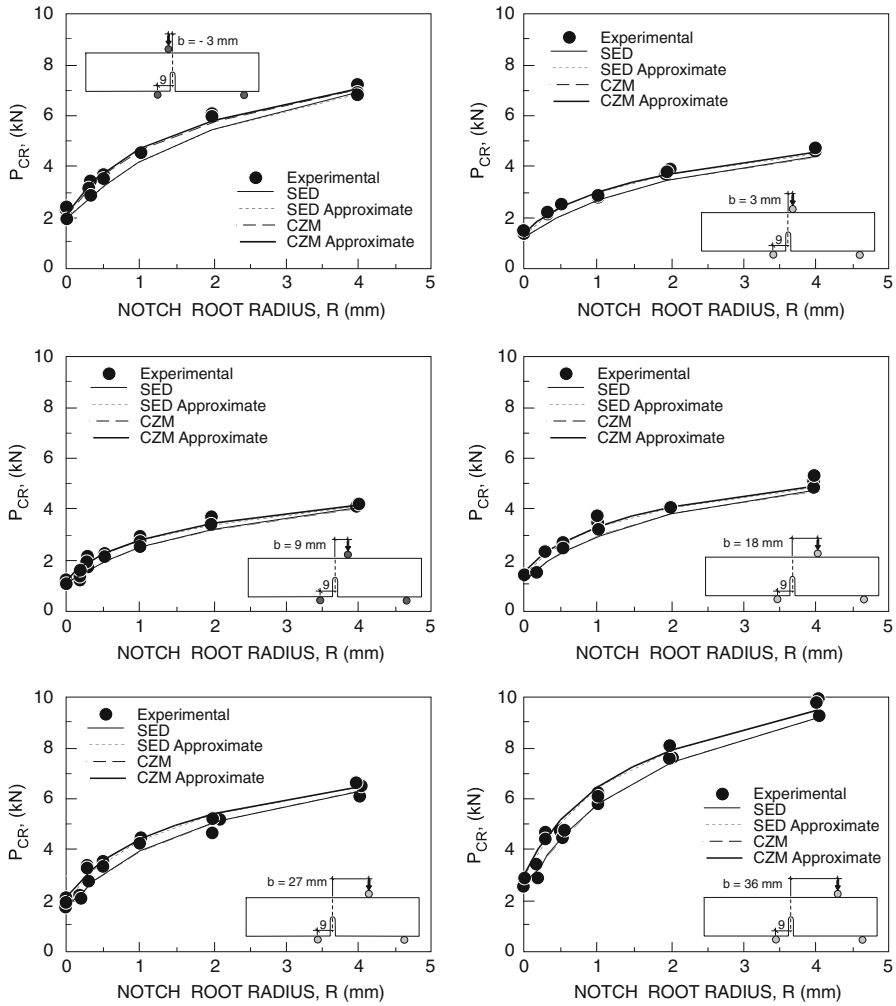

Fig. 12 Comparison between experimental and predicted values of the critical load for different notch root radii ($b = -3$, 3, 9, 18, 27 and 36 mm)

for the CZM model. For the latter, the differences in terms of critical loads between the predictions based on the numerical and the 'approximate' procedure, Eq. 23, are less than 5%.

The main differences between numerical and approximates procedures are in the last series corresponding to tilted notches with m = 3 mm. In these tests, fracture starts far from the notch tip, near the end of the circular contour. The influence of the straight contour of the notch could be one of the reasons for the discrepancy.

6 Summary and final comments

In this paper two different fracture criteria, based on the averaged strain energy density over a control volume and the cohesive zone model, have been generalised from mode I to mixed mode (I+II), under the hypothesis of an *equivalent local mode I* along the normal line to the notch edge, at a point where the principal stress reaches its maximum value. The two different approaches have been used to assess rupture loads of U-notched components made of PMMA and tested at −60°C under mixed mode loading.

The idea behind the equivalent local mode I is that the control volume, which was symmetric with respect to notch bisector line under Mode I loading, is shifted along the notch edge and centred with respect to the point of maximum principal stress. Since the influence of remaining stress components ($\sigma_{rr}, \sigma_{r\theta}$) is small in the presence of a blunt notch and near the control area, the hypothesis of an *equivalent local mode I* for mixed mode loading can be substantiated.

To check the proposed fracture criteria, a significant amount of experimental data, recently obtained by the authors, has been reconsidered. The measured critical loads have been compared with those obtained

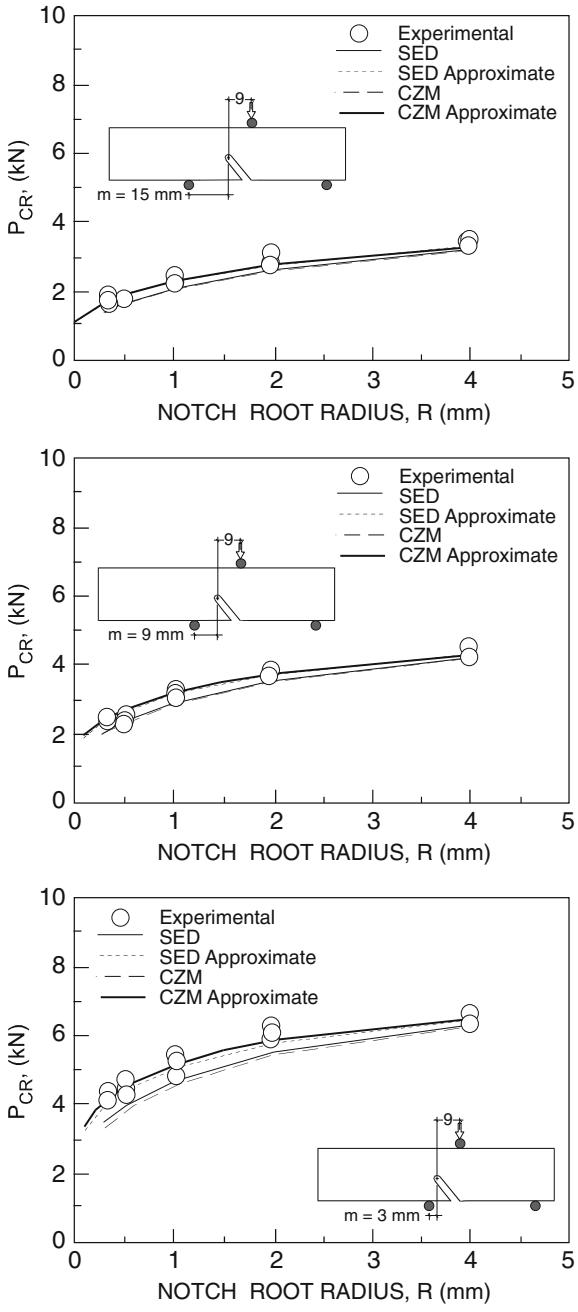

Fig. 13 Comparison between experimental and predicted values of the critical load for different notch root radii ($m = 15$, 9 and 3 mm)

numerically by means of the two approaches with a satisfactory agreement being found in all cases. This agreement between numerical and experimental values supports the hypothesis of local mode I. In all cases the divergences between each are of the same order than those that appear in previous analyses in which

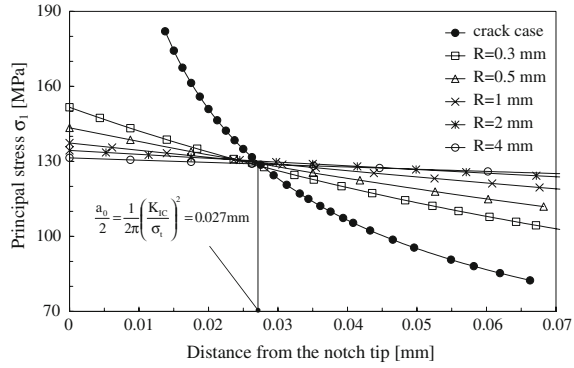

Fig. 14 Principal stress distribution along the normal line to the notch at the point where fracture starts. The figure has been obtained by imposing a constant value the strain energy density (1.69 Nmm/mm^3) on the control volume with a critical radius equal to 0.035 mm

only mode I was considered, (see Gómez et al. 2005 or Lazzarin and Berto 2005a).

An additional argument that supports the local mode I is the similitude between the stress fields shown in Figs. 5, 6 and 7. The only difference between the stress and energy contours from one geometry to another is the position of the point where the stress is at a maximum.

Figure 14 shows that for different notch radii the distribution of the principal stress σ_{11}, along the line which represents the axis of symmetry of the rotated control volume under mixed mode loading. The diagram has been obtained by imposing a constant value of the strain energy density ($W_c = 1.69\,\text{Nmm/mm}^3$) over the control volume having a critical radius R_c equal to 0.035 mm. The curves intersect each other at a distance approximately equal to $0.5a_0$, where a_0 is the extensively known El Haddad Smith Topper parameter (El Haddad et al. 1979) (the expression $R_c = 0.63a_0$ under plane strain conditions is valid for $\nu = 0.4$). Such a finding strongly supports the idea of the equivalent local mode I approach proposed in this study, confirming the fact that the critical radius R_c needs not be updated under mixed mode conditions (I+II) with respect to pure mode I loading.

Acknowledgments Support for this research was provided by the Spanish Ministerio de Ciencia y Tecnología under grants MAT2000-1355, MAT2001-3863-C03-01 and ENE2005-06478. The present work was conducted within the framework provided by the projects DUMEINPA (S-0505/MAT-0155) sponsored by the Regional Government of Madrid, Spain, and SEDUREC, integrated in the Spanish national research program CONSOLIDER-INGENIO 2010.

Appendix

Table A1 Outline of experimental values of the critical loads from beams with straight notches

R (mm)	b (mm)	P_1 (N)	P_2 (N)	P_3 (N)	<P> (N)
4	−3	6903	6830	7277	7003
	3	4716	4643	4645	4668
	9	4219	41550	4171	4182
	18	4885	5304	5133	5107
	27	6114	6518	6659	6430
	36	9968	9889	9286	9714
2	−3	5954	6093	6033	6027
	3	3880	3740	3775	3798
	9	3692	3700	3374	3589
	18	4079	4102	4062	4081
	27	5258	5210	4689	5052
	36	7606	7640	8113	7786
1	−3	4634	4633	4549	4605
	3	2901	2876	2846	2874
	9	2742	2886	2559	2729
	18	3531	3739	3262	3511
	27	4302	4401	4469	4391
	36	6242	6115	5835	6064
0.5	−3	3687	3682	3505	3625
	3	2530	2514	2562	2535
	9	2131	2246	2186	2188
	18	2504	2503	2677	2561
	27	3412	3509	3452	3458
	36	4837	4791	4519	4716
0.3	−3	3462	2880	3161	3168
	3	2146	2235	2195	2192
	9	1797	1918	2131	1949
	18	2356	2346	2345	2349
	27	3305	2776	3435	3172
	36	4722	4700	4487	4636
0.2	9	1427	1304	1193	1308
	18	1536	1528	1580	1548
	27	2097	2114	2171	2127
	36	3466	3486	2914	3289
0	−3	2213	1967	2426	2202
	3	1393	1486	1379	1419
	9	1136	1203	–	1170
	18	1507	1451	1418	1459
	27	1995	1785	2089	1956
	36	2582	2624	2933	2713

Table A2 Outline of experimental values of the critical loads from beams with inclined notches

R (mm)	w_1 (mm)	P_1 (N)	P_2 (N)	P_3 (N)	<P> (N)
4	15	3433	3329	3466	3409
	9	4225	4209	4448	4294
	3	6613	6337	6353	6434
2	15	2842	2809	3112	2921
	9	3743	3854	3729	3775
	3	6316	6086	5914	6105
1	15	2266	2310	2460	2345
	9	3327	3164	3008	3166
	3	5435	4851	5316	5201
0.5	15	1792	1783	1776	1784
	9	2323	2494	2436	2418
	3	4503	4732	4334	4523
0.3	15	1736	1866	1669	1757
	9	2397	2420	2446	2421
	3	4394	4354	4173	4307

Table A3 Outline of numerical results for straight notches

R (mm)	b (mm)	$\sigma^*_{\theta\theta}$ (MPa)	σ^*_{max} (MPa)	$K_1^{V,R}$ (MPa$\sqrt{m}$)	$K_2^{V,R}$ (MPa$\sqrt{m}$)	SED (MJ/m^3)
4	−3	145.75	146.38	7.90	−2.81	1.73
	3	135.38	154.10	7.38	−6.83	1.92
	9	110.81	149.36	6.20	−7.91	1.80
	18	105.18	155.05	5.88	−8.03	1.95
	27	99.76	147.33	5.57	−7.62	1.77
	36	103.93	152.13	5.82	−7.91	1.89
2	−3	157.18	161.30	6.14	2.31	2.05
	3	139.49	160.00	5.48	4.34	2.01
	9	123.10	161.87	4.87	−5.19	2.07
	18	109.57	155.30	4.33	−5.06	1.92
	27	102.33	145.14	4.05	−4.71	1.67
	36	108.56	152.94	4.30	−4.96	1.86
1	−3	158.09	164.10	4.40	−1.68	2.03
	3	140.23	160.95	3.91	−2.76	1.95
	9	125.69	162.67	3.51	−3.32	2.00
	18	127.44	175.96	3.57	−3.73	2.37
	27	120.20	166.06	3.35	−3.52	2.08
	36	114.23	156.85	3.19	−3.29	1.87
0.5	−3	165.45	175.75	3.32	−1.29	2.12
	3	167.83	193.28	3.33	−2.20	2.58
	9	138.46	177.27	2.75	−2.40	2.18
	18	128.49	174.17	2.56	−2.47	2.11
	27	130.83	177.44	2.59	−2.53	2.19
	36	122.62	165.27	2.43	−2.37	1.91

Table A3 continued

R (mm)	b (mm)	$\sigma^*_{\theta\theta}$ (MPa)	σ^*_{max} (MPa)	$K_1^{V,R}$ (MPa$\sqrt{m}$)	$K_2^{V,R}$ (MPa$\sqrt{m}$)	SED (MJ/m^3)
0.3	−3	185.27	194.53	2.79	−1.13	2.35
	3	184.94	211.85	2.79	−1.84	2.78
	9	157.26	200.19	2.40	−2.02	2.47
	18	150.85	202.44	2.31	−2.18	2.52
	27	153.62	206.28	2.37	−2.21	2.47
	36	154.33	206.19	2.37	−2.21	2.62
0.2	9	128.51	162.99	1.61	−1.33	1.44
	18	121.26	161.73	1.52	−1.39	1.44
	27	125.63	167.62	1.58	−1.45	1.52
	36	133.49	177.27	1.68	−1.52	1.70
0	−3	–	–	1.74	−0.40	2.05
	3	–	–	1.65	−0.58	2.15
	9	–	–	1.34	−0.61	1.70
	18	–	–	1.35	−0.68	1.88
	27	–	–	1.36	−0.68	1.92
	36	–	–	1.29	−0.65	1.73

Table A4 Outline of numerical results for inclined notches

R (mm)	w_1 (mm)	$\sigma^*_{\theta\theta}$ (MPa)	σ^*_{max} (MPa)	$K_1^{V,R}$ (MPa$\sqrt{m}$)	$K_2^{V,R}$ (MPa$\sqrt{m}$)	SED (MJ/m^3)
4	15	31.14	153.79	1.73	6.05	1.91
	9	−10.32	148.72	−0.41	6.88	1.78
	3	−102.00	148.16	−5.32	9.61	1.75
2	15	50.89	163.00	2.14	4.80	2.08
	9	7.47	158.16	0.48	5.41	1.96
	3	−104.11	163.67	3.87	8.31	2.06
1	15	33.05	168.43	1.99	−3.63	2.13
	9	22.96	166.80	0.80	−4.21	2.07
	3	−102.37	169.58	−2.69	−6.54	2.06
0.5	15	78.39	169.87	1.64	−2.66	1.98
	9	34.35	165.14	0.79	−3.07	1.83
	3	−108.96	185.65	−2.03	−5.39	2.18
0.3	15	104.03	208.95	1.68	−2.58	2.65
	9	50.71	203.45	0.87	−3.02	2.44
	3	−123.50	212.98	−1.80	−5.00	2.56

$\sigma^*_{\theta\theta}$ is the stress on the notch tip along the notch bisector line

σ^*_{max} is the maximum stress out of the notch bisector line

$K_1^{V,R}$ and $K_2^{V,R}$ are the generalized stress intensity factor evaluated by using the definition by Lazzarin and Filippi (2006)

$$K_1^{V,R} = \sqrt{2\pi}\frac{(\sigma_{\theta\theta})_{\theta=0} r^{1-\lambda_1}}{1+\tilde{\omega}_1\left(\frac{r}{r_0}\right)^{\mu_1-\lambda_1}} \quad K_2^{V,R} = \sqrt{2\pi}\frac{(\tau_{r\theta})_{\theta=0} r^{1-\lambda_2}}{1+\tilde{\omega}_2\left(\frac{r}{r_0}\right)^{\mu_2-\lambda_2}} \tag{A1}$$

SED is the value of the energy averaged over the control volume of radius R_c

Please note that the results related to the straight notches (with b = 9, 18, 27, 36) are reported also in the paper by Gomez et al. 2007

References

Atzori B, Lazzarin P (2001) Notch sensitivity and defect sensitivity: two sides of the same medal. Int J Fract 107(1):L3–L8

Atzori B, Lazzarin P, Meneghetti G (2003) Fracture mechanics and notch sensitivity. Fatigue Fract Eng Mater Struct 26:257–267

Atzori B, Lazzarin P, Meneghetti G (2005) Unified treatment of fatigue limit of components weakened by notches and defects subjected to prevailing mode I stresses. Int J Fract 133:61–87

Barenblatt GI (1962) The mathematical theory of equilibrium of cracks in brittle fracture. Adv Appl Mech 7:55–129

Bažant ZP, Planas J (1998) Fracture and size effect in concrete and other quasibrittle materials. CRC Press, Boca Raton and London

Berto F, Lazzarin P (2007) Relationships between J-integral and the strain energy evaluated in a finite volume surrounding the tip of sharp and blunt V-notches. Int J Solids Struct 44:4621–4645

Berto F, Lazzarin P, Matvienko YUG (2007) J-integral evaluation for U- and V-blunt notches under Mode I loading and materials obeying a power hardening law. Int J Fract 146:33–51

Budiansky B, Rice JR (1973) Conservation laws and energy-release rate. J Appl Mech 40:201–203

Carpinteri A (1987) Stress singularity and generalised fracture toughness at the vertex of re-entrant corners. Eng Fract Mech 26:143–155

Chen YH, Lu TJ (2004) On the path dependence of the J-integral in notch problems. Int J Solids Struct 41:607–618

Creager M, Paris PC (1967) Elastic field equations for blunt cracks with reference to stress corrosion cracking. Int J Fract Mech 3:247–252

Czoboly E, Havas I, Gillemot F (1982) The absorbed specific energy till fracture as a measure of the toughness of metals. In Sih GC, Czoboly E, Gillemot F (eds) Proceedings of international symposium on absorbed specific energy and/or strain energy density. Martinus Nijhoff, The Hague, pp 101–106

Dini D, Hills D (2004) Asymptotic characterisation of nearly-sharp notch root stress fields. Int J Fract 130:651–666

Dugdale DS (1960) Yielding of steel sheets containing slits. J Mech Phys Solids 8:100–108

El Haddad MH, Topper TH, Smith KN (1979) Prediction of non-propagating cracks. Eng Fract Mech 11:573–584

Elices M, Guinea GV, Gómez FJ, Planas J (2002) The cohesive zone model: advantages, limitations and challenges. Eng Fract Mech 69:137–163

Ellyin F (1997) Fatigue damage, crack growth and life prediction. Chapman & Hall, London

Ellyin F, Kujawski D (1989) Generalization of notch analysis and its extension to cyclic loading. Eng Fract Mech 32(5):819–826

Erdogan F, Sih CG (1963) On the crack extension in plates under plane loading and transverse shear. J Basic Eng 519–525

Gdoutos EE (1990) Fracture mechanics criteria and applications. Kluwer Academic Publishers, Dodrecht

Gillemot EE (1965) Brittle fracture of welded materials. Commonwealth Welding Conference C 7:353–358

Gillemot LF (1976) Criterion of crack initiation and spreading. Eng Fract Mech 8:239–253

Gillemot LF, Czoboly E, Havas I (1985) Fracture mechanics applications of absorbed specific fracture energy: notch and unnotched specimens. Theor Appl Fract Mech 4:39–45

Gogotsi GA (2003) Fracture toughness of ceramics and ceramic composites. Ceram Int 7:777–884

Gómez FJ, Elices M (2003a) Fracture of components with V-shaped notches. Eng Fract Mech 70:1913–1927

Gómez FJ, Elices M (2003b) A fracture criterion for sharp V-notched samples. Int J Fract 123:163–175

Gómez FJ, Elices M (2004) A fracture criterion for blunted V-notched samples. Int J Fract 127:239–264

Gómez FJ, Elices M, Valiente A (2000) Cracking in PMMA containing U-shaped notches. Fatigue Fract Eng Mat Struct 23:795–803

Gómez FJ, Elices M, Planas J (2005) The cohesive crack concept: application to PMMA at −60°C. Eng Fract Mech 72:1268–1285

Gómez FJ, Elices M, Berto F, Lazzarin P (2007a) Local strain energy to asses the static failure of U-notches in plates under mixed mode loading. Int J Fract 145:29–45

Gómez FJ, Elices M, Berto F, Lazzarin P (2007b) Fracture of U-notched specimens under mixed mode experimental results and numerical predictions. Eng Fract Mech (in press)

Hillerborg A, Modéer M, Petersson PE (1976) Analysis of crack formation and crack growth in concrete by means of fracture mechanics and finite elements. Cement Concrete Res 6:773–782

Kipp ME, Sih GC (1975) The strain energy density failure criterion applied to notched elastic solids. Int J Solids Struct 11:153–173

Knésl Z (1991) A criterion of V-notch stability. Int J Fract 48:R79–R83

Knowles JK, Sternberg E (1972) On a class of conservation laws in linearized and finite elastostatics. Arch Rational Mech Anal 44:187–211

Lazzarin P, Tovo R (1996) A unified approach to the evaluation of linear elastic stress fields in the neighbourhood of cracks and notches. Int J Fract 78:3–19

Lazzarin P, Zambardi R (2001) A finite-volume-energy based approach to predict the static and fatigue behaviour of components with sharp V-shaped notches. Int J Fract 112: 275–298

Lazzarin P, Berto F (2005a) Some expressions for the strain energy in a finite volume surrounding the root of blunt V-notches. Int J Fract 135:161–185

Lazzarin P, Berto F (2005b) From Neuber's elementary volume to Kitagawa and Atzori's diagrams: an interpretation based on local energy. Int J Fract 135:L33–L38

Lazzarin P, Filippi S (2006) A generalised stress intensity factor to be applied to rounded V-shaped notches. Int J Solids Struct 43:2461–2478

Lazzarin P, Berto F (2008) Control volumes and strain energy density under small and large scale yielding due to tension and torsion loading. Fatigue Fract Eng Mater Struct 31: 95–107

Lazzarin P, Lassen T, Livieri P (2003) A Notch Stress Intensity approach applied to fatigue life predictions of welded joints with different local toe geometry. Fatigue Fract Eng Mater Struct 26:49–48

Lazzarin P, Sonsino CM, Zambardi R (2004) A notch stress intensity approach to predict the fatigue behaviour of T butt

welds between tube and flange when subjected to in-phase bending and torsion loading. Fatigue Fract Eng Mater Struct 27:127–141

Lazzarin P, Berto F, Radaj D (2006) Uniform fatigue strength of butt and fillet welded joints in terms of the local strain energy density. Proceedings 9th international fatigue congress, IFC9, Atlanta, USA (Organised by Elsevier). On CD Rom

Lazzarin P, Livieri P, Berto F, Zappalorto M (2008) Local strain energy density and fatigue strength of welded joints under uniaxial and multiaxial loading. Eng Fract Mech 75:1875–1889

Leguillon D, Yosibash Z (2003) Crack onset at a V-notch influence of the notch tip radius. Int J Fract 122:1–21

Leguillon D, Quesada D, Putot C, Martin E (2007) Prediction of crack initiation at blunt notches and cavities—size effects. Eng Fract Mech 74:2420–2436

Livieri P (2008) Use of J-integral to predict static failures in sharp V-notches and rounded U-notches. Eng Fract Mech 75:1779–1793

Livieri P, Lazzarin P (2005) Fatigue strength of steel and aluminium welded joints based on generalised stress intensity factors and local strain energy values. Int J Fract 133: 247–278

McClintock FA (1958) Ductile fracture instability in shear. J Appl Mech 25:582–588

Neuber H (1958) Kerbspannungslehre. 2. Springer-Verlag, Berlin

Neuber H (1985) Kerbspannungslehre. 3. Springer-Verlag, Berlin

Novozhilov VV (1969) On necessary and sufficient criterion of brittle fracture. Prikladnaja Matematika i Mechanika 33:212–222

Nui LS, Chehimi C, Pluvinage G (1994) Stress field near a large blunted tip V-Notch and application of the concept of the critical notch stress intensity factor (NSIF) to the fracture toughness of very brittle materials. Eng Fract Mech 49: 325–335

Papadopoulos GA, Paniridis PI (1988) Crack initiation from blunt notches under biaxial loading. Eng Fract Mech 31(1):65–78

Planas J, Sancho JM (2007) Computational Orientated Finite Elements. COFE. Internal report. JP0501. Departamento de Ciencia de los Materiales. Universidad Politécnica de Madrid

Priel E, Bussiba A, Gilad I, Yosibash Z (2007) Mixed mode failure criteria for brittle elastic V-notched structures. Int J Fract 144:247–265

Rice JR (1968) A path independent integral and the approximate analysis of strain concentration by notches and cracks. J Appl Mech 35:379–386

Ritchie RO, Knott JF, Rice JR (1973) On the relation between critical tensile stress in fracture toughness in mild steel. J Mech Phys Solids 21:395–410

Sancho JM, Planas J, Cendón DA, Reyes E, Gálvez JC (2007) An embedded crack model for finite element analysis of concrete fracture. Eng Fract Mech 74:75–86

Seweryn A (1994) Brittle fracture criterion for structures with sharp notches. Eng Fract Mech 47:673–681

Seweryn A, Mróz Z (1995) A non-local stress failure condition for structural elements under multiaxial loading. Eng Fract Mech 51:955–973

Seweryn A, Lucaszewicz A (2002) Verification of brittle fracture criteria for elements with V-shaped notches. Eng Fract Mech 69:1487–1510

Seweryn A, Poskrobko S, Mróz Z (1997) Brittle fracture in plane elements with sharp notches under mixed-mode loading. J Eng Mech 123:535–543

Sheppard SD (1991) Field effects in fatigue crack initiation: long life fatigue strength. Trans ASME J Mech Design 113: 188–194

Sih GC (1973) A special theory of crack propagation. In: Sih GC (ed) Methods of analysis and solutions of crack problems. Noordhoff, International Publishing, Leyden, pp 21–45

Sih GC (1974a) Strain-energy-density factor applied to mixed mode crack problems. Int J Fract 10:305–321

Sih GC (1974b) Surface layer energy and strain energy density for a blunted crack or notch. In: Sih GC, van Elst HC, Broek D (eds) Prospect of fracture mechanics. Noordhoff International Publishing, Leyden, pp 85–102

Sih GC (1991) Mechanics of fracture initiation and propagation: surface and volume energy density applied as failure criterion. Kluwer Academic Publisher, Dordrecht

Strandberg M (2002) Fracture at V-notches with contained plasticity. Eng Fract Mech 69:403–415

Taylor D (2004) Predicting the fracture strength of ceramic materials using the theory of critical distances. Eng Fract Mech 71:2407–2416

Yosibash Z, Bussiba Ar, Gilad I (2004) Failure criteria for brittle elastic materials. Int J Fract 125:307–333

Yosibash Z, Priel E, Leguillon D (2006) A failure criterion for brittle elastic materials under mixed-mode loading. Int J Fract 141:291–312